

Limited-control optimal protocols arbitrarily far from equilibrium

Adrienne Zhong^{1,*} and Michael R. DeWeese^{1,2}

¹*Department of Physics, University of California, Berkeley, Berkeley, CA, 94720*

²*Redwood Center For Theoretical Neuroscience and Helen Wills Neuroscience Institute, University of California, Berkeley, Berkeley, CA, 94720*

**Corresponding author: adrzhong@berkeley.edu*

May 19, 2022

Abstract

Optimizing the energy efficiency of finite-time processes is of major interest in the study of non-equilibrium systems. Recent studies have explored finite-time dissipation-minimizing protocols for stochastic thermodynamic systems driven arbitrarily far from equilibrium, when granted full external control to drive the system. However, often times in both simulation and experimental contexts, systems may only be controlled with a limited set of degrees of freedom. Here, we apply ideas from optimal control theory to obtain optimal protocols arbitrarily far from equilibrium for this unexplored limited-control setting. By working with deterministic Fokker-Planck probability distribution time evolution and using the first law of thermodynamics to recast the work-expenditure, we can frame the work-minimizing protocol problem in the standard form of an optimal control theory problem. We demonstrate that finding the exact optimal protocol is equivalent to solving a system of Hamiltonian partial differential equations, which in many cases admit efficiently calculatable numerical solutions. Within this framework, we reproduce analytical results for the optimal control of harmonic potentials, and numerically devise novel optimal protocols for two examples: varying the stiffness of a quartic potential, and linearly biasing a double-well potential. We confirm that these optimal protocols outperform other protocols produced through previous methods, in some cases by a significant amount. We find that for the linearly biased double-well problem, the mean position under the optimal protocol travels at a near-constant velocity, and that surprisingly, for a certain timescale and barrier height regime, the optimal protocol is non-monotonic in time.

1 Introduction

There has been much recent progress in the study of non-equilibrium stochastic thermodynamics [1, 2, 3]. In particular, optimal finite-time protocols have been derived for a variety of systems, with applications to finite-time free-energy difference estimation [4, 5, 6] engineering optimal bit erasure [7, 8], and the design of optimal nanoscale heat engines [9, 10, 11].

For finite-time dissipation-minimizing protocols, there are two related optimization problems that are typically studied: designing protocols that transition between two specified distributions within finite time that minimize entropy production [12, 13, 14, 15], and designing protocols that minimize the amount work needed to shift between two different potential energy landscapes within finite time [4, 16]. For the first

problem, methods have been devised to fully control probability density evolution arbitrarily far from equilibrium [17, 18, 19], establishing deep ties with optimal transport theory [12, 20, 13] and culminating in the derivation of an absolute geometric lower bound for finite-time entropy production in terms of the L^2 -Wasserstein distance [13, 14, 15, 21]. Crucially, however, full control over the potential energy is needed to satisfy arbitrarily specified initial and terminal conditions in these types of problems.

Here, we consider the second problem for the case in which there is only limited, finite-dimensional control of the potential. Only for the simplest case of a Brownian particle in a harmonic potential has the fully non-equilibrium optimal protocol been analytically solved and studied [4, 12, 22, 23]. For arbitrary potentials, limited control optimal protocol approximations for the slow near-equilibrium $t_f \gg 1$ [16, 24, 25, 26] and the fast $t_f \ll 1$ [27] regimes have been derived, but these approximations generally are optimal only within the specified limits. Very recently, gradient methods have been devised to calculate fully non-equilibrium optimal protocols through sampling many stochastic trajectories [28, 29, 30].

In this work, we show that optimal control theory is a principled and powerful framework to derive exact optimal protocols for limited-control potentials arbitrarily far from equilibrium. Optimal control theory (OCT), having roots in Lagrange’s calculus of variations, is a well-studied field of applied mathematics that deals with finding controls of a dynamical system that optimize a specified objective function, with numerous applications to science and engineering [31, 32]. By working directly with the probability density undergoing deterministic Fokker-Planck dynamics (as opposed to individual stochastic trajectories), and rewriting the objective function using the first law of thermodynamics, we show that the problem of finding optimal protocols can be recast in the standard OCT problem form. We may then apply Pontryagin’s maximum principle, one of OCT’s foundational theorems, to yield Hamiltonian partial differential equations whose solutions directly give optimal protocols. We note that the optimal control of fields and stochastic systems has been previously studied within applied mathematics and engineering literature [33, 34, 35, 36, 37, 38, 39, 40, 41, 42], but to our knowledge it has never been used to derive exact optimal work-minimizing protocols in stochastic thermodynamics.

An outline of this paper is as follows. First, we use OCT to derive Hamiltonian partial differential equations whose solutions give optimal protocols for the cases of Markov jump processes over discrete states and Langevin dynamics over continuous configuration space. We then solve these equations analytically for harmonic potential control to reproduce known optimal protocols. Finally, we describe and use a computationally efficient algorithm to numerically calculate optimal protocols for two anharmonic examples: controlling the stiffness of a quartic trap, and linearly biasing a quartic double-well potential. We demonstrate the superiority in performance of these optimal protocols compared to the protocols derived through approximation methods. We discover that for the linearly biased double-well problem, the mean position travels with near-constant velocity under the optimal protocol, and that certain optimal protocols have a remarkably counter-intuitive property — the control parameter is non-monotonic in time within a certain time and barrier height parameter regime. Finally, we discuss our findings and the implications of our work for the study of non-equilibrium stochastic thermodynamics.

2 Derivation for discrete state case

We start by considering a continuous-time Markov jump process with d discrete states. The experimenter has control over the protocol parameter $\lambda(t)$ that determines the potential energies of the states, encoded by the vector $\mathbf{U}_\lambda = (U_1(\lambda), U_2(\lambda), \dots, U_d(\lambda))^T$. Here λ is single parameter, but in general it can be multi-

dimensional. Although an individual jump process trajectory is stochastic, the time-varying probability distribution over states, represented by the vector $\boldsymbol{\rho}(t) = (\rho^1, \rho^2, \dots, \rho^d)^T$ with $\sum_i \rho^i = 1$, has deterministic dynamics governed by a master equation

$$\dot{\boldsymbol{\rho}} = \mathcal{L}_\lambda \boldsymbol{\rho}, \quad (1)$$

where \mathcal{L}_λ is a transition rate matrix for which we impose the following form (similar to [43])

$$[\mathcal{L}_\lambda]_{ij}^i = \begin{cases} c_{ij} e^{\beta(U_j(\lambda) - U_i(\lambda))/2} & i \neq j \\ -\sum_{k \neq j} c_{kj} e^{\beta(U_j(\lambda) - U_k(\lambda))/2} & i = j. \end{cases} \quad (2)$$

Here $\beta = 1/k_B T$ is the inverse temperature, k_B is the Boltzmann constant, and $c_{ij} = c_{ji}$ is the symmetric non-negative connectivity strength between distinct states $i \neq j$. Transition rate matrices have the property $\sum_i [\mathcal{L}_\lambda]_{ij}^i = 0$, ensuring conservation of total probability. In particular, this matrix \mathcal{L}_λ satisfies the detailed-balance condition $[\mathcal{L}_\lambda]_{ij}^i \rho_{\text{eq},\lambda}^j = [\mathcal{L}_\lambda]_{ji}^j \rho_{\text{eq},\lambda}^i$ for all i and j , where $\rho_{\text{eq},\lambda}^i \propto e^{-\beta U_i(\lambda)}$ is the unique Boltzmann equilibrium distribution for \mathbf{U}_λ .

For time-varying $\lambda(t)$ and $\boldsymbol{\rho}(t)$, the ensemble-averaged energy is $E(t) = \mathbf{U}_\lambda^T \boldsymbol{\rho}$ and has time derivative

$$\dot{E} = \dot{\lambda} \left[\frac{d\mathbf{U}_\lambda}{d\lambda} \right]^T \boldsymbol{\rho} + \mathbf{U}_\lambda^T \dot{\boldsymbol{\rho}}. \quad (3)$$

As is customary in stochastic thermodynamics, the first term in the sum is interpreted as the rate of work applied to the system \dot{W} , and the second term the rate of heat in from the heat bath \dot{Q} [44].

We would like to solve the following optimization problem: if at $t = 0$ we start at the equilibrium distribution $\boldsymbol{\rho}_{\text{eq},i}$ for potential energy \mathbf{U}_{λ_i} , what is the optimal finite-time protocol $\lambda(t)$ that terminates at λ_f at final time $t = t_f$, and minimizes the work

$$W[\lambda(t)] = \int_0^{t_f} \dot{\lambda} \left\langle \frac{\partial U}{\partial \lambda} \right\rangle dt = \int_0^{t_f} \dot{\lambda} \left[\frac{d\mathbf{U}_\lambda}{d\lambda} \right]^T \boldsymbol{\rho} dt? \quad (4)$$

We emphasize that this time integral includes any discontinuous jumps of λ that may occur at the beginning and end of the protocol, which has been shown to be a common feature for finite-time optimal protocols [4, 45, 5]. Note that in general, $\boldsymbol{\rho}(t_f) \neq \boldsymbol{\rho}_{\text{eq},f}$ the equilibrium distribution corresponding to λ_f .

The first law of thermodynamics $\Delta E[\lambda(t)] = W[\lambda(t)] + Q[\lambda(t)]$ allows us to write

$$\begin{aligned} W[\lambda(t)] &= (\mathbf{U}_f^T \boldsymbol{\rho}(t_f) - \mathbf{U}_i^T \boldsymbol{\rho}(0)) - \int_0^{t_f} \mathbf{U}_\lambda^T \dot{\boldsymbol{\rho}} dt \\ &= (\mathbf{U}_f - \mathbf{U}_i)^T \boldsymbol{\rho}_{\text{eq},i} + \int_0^{t_f} (\mathbf{U}_f - \mathbf{U}_\lambda)^T \mathcal{L}_\lambda \boldsymbol{\rho} dt. \end{aligned} \quad (5)$$

Here, $\mathbf{U}_i = \mathbf{U}_{\lambda_i}$, and $\mathbf{U}_f = \mathbf{U}_{\lambda_f}$. In the second line, we use $\boldsymbol{\rho}(t_f) = \boldsymbol{\rho}(0) + \int_0^{t_f} \dot{\boldsymbol{\rho}} dt$, and invoke (1). The first term in the sum is protocol independent, so minimizing $W[\lambda(t)]$ is akin to minimizing the second term

$$J[\lambda(t)] = \int_0^{t_f} (\mathbf{U}_f - \mathbf{U}_\lambda)^T \mathcal{L}_\lambda \boldsymbol{\rho} dt, \quad (6)$$

which is now in the form of the fixed-time, free-endpoint Lagrange problem in optimal control theory [31]. Compared to a typical Euler-Lagrange calculus of variations problem in classical physics [46, 47], here both

the initial state $\boldsymbol{\rho}(t = 0) = \boldsymbol{\rho}_{\text{eq},i}$ and the time interval $[0, t_f]$ are specified, but notably, the final state $\boldsymbol{\rho}(t = t_f)$ is unconstrained.

The standard OCT solution derivation begins by expanding the integrand of (6) with Lagrange multipliers $\boldsymbol{\pi}(t) = (\pi_1, \pi_2, \dots, \pi_d)^T$

$$L = (\mathbf{U}_f - \mathbf{U}_\lambda)^T \mathcal{L}_\lambda \boldsymbol{\rho} + \boldsymbol{\pi}^T (\dot{\boldsymbol{\rho}} - \mathcal{L}_\lambda \boldsymbol{\rho}), \quad (7)$$

so that the desired dynamics (1) are ensured. A solution $[\boldsymbol{\rho}^*(t), \boldsymbol{\pi}^*(t), \lambda^*(t)]$ that minimizes $\int_0^{t_f} L dt$ gives the optimal protocol $\lambda^*(t)$ that minimizes $J[\lambda(t)]$.

A Legendre transform $H = \boldsymbol{\pi}^T \dot{\boldsymbol{\rho}} - L$ produces the control-theoretic Hamiltonian

$$H(\boldsymbol{\rho}, \boldsymbol{\pi}, \lambda) = (\boldsymbol{\pi} + \mathbf{U}_\lambda - \mathbf{U}_f)^T \mathcal{L}_\lambda \boldsymbol{\rho}, \quad (8)$$

where $\boldsymbol{\pi}$ may now be interpreted as the conjugate momentum to $\boldsymbol{\rho}$. Pontryagin's maximum principle gives necessary conditions for an optimal solution $[\boldsymbol{\rho}^*(t), \boldsymbol{\pi}^*(t), \lambda^*(t)]$: it must satisfy the canonical equations $\dot{\rho}^i = \partial H / \partial \pi_i$ and $\dot{\pi}_i = -\partial H / \partial \rho_i$ for $i = 1, 2, \dots, d$, and constraint equation $\partial H / \partial \lambda = 0$, with $\partial^2 H / \partial \lambda^2 < 0$ along the optimal protocol. Because Eq. (8) has no explicit time dependence, it remains constant throughout an optimal protocol. Although this is in a sense analogous to the conserved total energy in a classical system, it does not apparently represent a physical energy of the system [31].

From Pontryagin's maximum principle, the canonical equations for the Hamiltonian in Eq. (8) are

$$\dot{\boldsymbol{\rho}} = \mathcal{L}_\lambda \boldsymbol{\rho} \quad (9)$$

$$\dot{\boldsymbol{\pi}} = -\mathcal{L}_\lambda^T (\boldsymbol{\pi} + \mathbf{U}_\lambda - \mathbf{U}_f), \quad (10)$$

while the constraint equation coupling the two canonical equations is

$$\left(\left[\frac{d\mathbf{U}_\lambda}{d\lambda} \right]^T \mathcal{L}_\lambda + (\boldsymbol{\pi} + \mathbf{U}_\lambda - \mathbf{U}_f)^T \frac{d\mathcal{L}_\lambda}{d\lambda} \right) \boldsymbol{\rho} = 0. \quad (11)$$

Because $\boldsymbol{\rho}(t_f)$ is unconstrained, the transversality condition fixes the terminal conjugate momentum $\boldsymbol{\pi}(t_f) = \mathbf{0}$ [31].

We have arrived at our first major contribution in this manuscript. For a discrete state Markov jump process, Pontryagin's maximum principle allows us to find the work-minimizing optimal protocol $\lambda^*(t)$ by solving the canonical differential Eqs. (9) and (10) coupled by Eq. (11), with the mixed boundary conditions $\boldsymbol{\rho}(0) = \boldsymbol{\rho}_i$, $\boldsymbol{\pi}(t_f) = \mathbf{0}$. Notably, no approximations have been used here, and thus the optimal protocols produced within this framework are exact for any time-scale. As will be shown below, efficient algorithms may be written to numerically solve these ordinary differential equations. This will be useful for numerically solving for optimal protocols of a continuous-state stochastic system, as continuous-state Fokker-Planck dynamics may be approximated by a discrete state Markov process with the appropriate master equation [48, 49]. All that remains in our derivation is to take the continuum limit for the corresponding result for a continuous stochastic system undergoing Langevin dynamics.

3 Continuous-state optimal protocol

For a continuous-state overdamped system in one dimension, individual trajectories undergo dynamics given by the Langevin equation

$$\dot{x} = -\beta D \frac{\partial U}{\partial x} + \eta(t). \quad (12)$$

Here D is the diffusion coefficient, $U(x, \lambda)$ is the λ -controlled potential, and $\eta(t)$ is Gaussian white noise with statistics $\langle \eta(t)\eta(t') \rangle = 2D\delta(t-t')$.

While each individual trajectory is stochastic, the time evolution of the probability density $\rho(x, t)$ of the ensemble is deterministic, given by a Fokker-Planck equation

$$\frac{\partial \rho}{\partial t} = D \left[\frac{\partial^2 \rho}{\partial x^2} + \beta \frac{\partial}{\partial x} \left(\rho \frac{\partial U}{\partial x} \right) \right] =: \hat{\mathcal{L}}_\lambda \rho, \quad (13)$$

Here, $\hat{\mathcal{L}}_\lambda$ denotes the Fokker-Planck operator, which has a corresponding adjoint operator $\mathcal{L}_\lambda^\dagger$, also known as the backward Kolmogorov operator [50, 49], that acts on a function $\psi(x, t)$ as

$$\mathcal{L}_\lambda^\dagger \psi := D \left[\frac{\partial^2 \psi}{\partial x^2} - \beta \frac{\partial \psi}{\partial x} \frac{\partial U}{\partial x} \right]. \quad (14)$$

Again, we want to find a protocol $\lambda(t)$ that minimizes the expected work

$$W[\lambda(t)] = \int_0^{t_f} \dot{\lambda} \left\langle \frac{\partial U}{\partial \lambda} \right\rangle dt, \quad (15)$$

beginning at $\lambda(0) = \lambda_i$ and $\rho(x, 0) \propto e^{-\beta U(x, \lambda_i)}$, and ending at $\lambda(t_f) = \lambda_f$ with $\rho(x, t_f)$ unconstrained.

To take the continuum limit of the discrete case, we treat the d states as 1-dimensional lattice sites with spacing Δx and reflecting boundaries at $x_b = \pm(d-1)\Delta x/2$, and set the connectivity coefficients of Eq. (2) to $c_{ij} = D(\Delta x)^{-2}$ for all pairs of neighboring sites $\{i, j\}$, s.t. $|i-j| = 1$, and $c_{ij} = 0$ for all else. We define $\rho(x, t) = (\Delta x)^{-1}[\rho(t)]^{l(x)}$, $\pi(x, t) = [\pi(t)]_{l(x)}$, and $U(x, \lambda) = [U_\lambda]_{l(x)}$, where $l(x) = \lfloor x/\Delta x + d/2 \rfloor$, and take the continuum limit $|x_b| \rightarrow \infty$ and $\Delta x \rightarrow 0$. Our control-theoretic Hamiltonian then becomes

$$H = \int_{-\infty}^{\infty} (\pi + U - U_f) \hat{\mathcal{L}}_\lambda \rho dx \quad (16)$$

with $U_f = U(x, \lambda_f)$, while the canonical Eqs. (9) and (10) become

$$\partial_t \rho = \hat{\mathcal{L}}_\lambda \rho \quad \text{and} \quad \partial_t \pi = -\hat{\mathcal{L}}_\lambda^\dagger (\pi + U - U_f). \quad (17)$$

Finally, under the continuum limit, the constraint Eq. (11) becomes

$$\int_{-\infty}^{\infty} \left[\frac{\partial U}{\partial \lambda} \right] \left(\hat{\mathcal{L}}_\lambda \rho + \beta D \frac{\partial}{\partial x} \left[\rho \frac{\partial}{\partial x} (\pi + U - U_f) \right] \right) dx = 0, \quad (18)$$

which may be interpreted as an orthogonality constraint between $\partial U/\partial \lambda$, and a Fokker-Planck operator with modified potential energy $\pi + 2U - U_f$ acting on ρ .

We have now derived an expression that allows us to find the work-minimizing optimal protocol for a

continuous-state stochastic system undergoing Langevin dynamics. Just as for the discrete case, solving Eqs. (17) and (18) with initial and terminal conditions $\rho(x, 0) = \rho_{\text{eq},i}(x)$ and $\pi(x, t_f) = 0$, gives us a principled way to find the optimal protocol $\lambda^*(t)$ that minimizes the work (15). Importantly, these differential equations are much more tractable than the generalized integro-differential equation proposed in [4] for finding the optimal protocol. In particular, these equations are solvable analytically for the control of harmonic potentials, and they may be efficiently solved numerically for the control of general anharmonic potentials.

For the rest of the paper we will consider affine-control potentials of the form

$$U(x, \lambda) = U_0(x) + \lambda U_1(x) + U_c(\lambda), \quad (19)$$

where λ linearly modulates the strength of an auxiliary potential $U_1(x)$ added to the base potential $U_0(x)$, modulo a constant offset U_c . This form is applicable to a wide class of experimental stochastic thermodynamics problems, including molecular pulling experiments [24, 51, 3, 18, 52] which can be modeled with potential $U(x, \lambda) = U_{\text{sys}}(x) + U_{\text{ext}}(x, \lambda)$ where the external potential of constant stiffness k is $U_{\text{ext}}(x, \lambda) = k(x - \lambda)^2/2$. We see that by expanding the square, this potential is in the form (19) with $U_0(x) = U_{\text{sys}}(x) + kx^2/2$, $U_1(x) = -kx$, and $U_c(\lambda) = k\lambda^2/2$.

By plugging (19) into (18), we see that for this class of affine-control potentials the constraint equation is invertible, giving

$$\lambda[\rho, \pi] = \frac{\lambda_f}{2} + \frac{\int_{-\infty}^{\infty} [\partial_x^2 U_1 - \beta(\partial_x U_1)(\partial_x(\pi + U_0))] \rho dx}{2 \int_{-\infty}^{\infty} (\partial_x U_1)^2 \rho dx}. \quad (20)$$

Plugging Eqs. (19) and (20) into (16) yields $\partial^2 H / \partial \lambda^2 = -2 \int (\partial_x U_1)^2 \rho dx < 0$, which demonstrates that the optimal protocol is a minimizing extremum for the work (6). A proof for the existence of optimal protocol solutions for Fokker-Planck optimal control is given in [34] under loose assumptions. While we currently cannot prove the uniqueness of a solution of Eqs. (17) and (20) with our mixed boundary conditions, every solution we have found always outperforms all other protocols we have considered.

We will now illustrate how Eqs. (17) and (20) can be used to produce optimal protocols, through particular analytical and numerical examples.

4 Harmonic trap with varied stiffness: an analytic example

For the rest of the paper, we set $D = \beta = 1$ for notational simplicity.

We start by considering a harmonic potential with λ controlling the stiffness of the potential $U(x, \lambda) = \lambda x^2/2$, where we identify $U_1 = x^2/2$ and $U_0 = U_c = 0$. It has been shown [4, 12] that when the probability distribution ρ starts as a Gaussian centered at zero, it remains a Gaussian centered at 0, with the dynamics of the inverse of the variance $s(t) = \langle x^2 \rangle^{-1}$ given by

$$\dot{s} = 2s(\lambda - s), \quad (21)$$

which can be obtained by plugging a zero-mean Gaussian ρ into Eq. (17).

By plugging a truncated polynomial ansatz for the conjugate momentum, $\pi(x, t) = \sum_{k=0}^n p_k(t) x^k / k!$, into Eq. (17) and taking into account our terminal condition $\pi(x, t_f) = 0$, we see that the only surviving terms are the constant and quadratic terms $\pi(x, t) = p_0(t) + p_2(t)x^2/2$, where the coefficients follow dynamics

given by

$$\dot{p}_0 = -(p_2 + \lambda - \lambda_f) \quad (22)$$

$$\dot{p}_2 = 2\lambda(p_2 + \lambda - \lambda_f). \quad (23)$$

From our constraint Eq. (20) we have

$$\lambda = \frac{\lambda_f}{2} + \frac{\int_{-\infty}^{\infty} (1 - p_2 x^2) \rho dx}{2 \int_{-\infty}^{\infty} x^2 \rho dx} = \frac{\lambda_f + s - p_2}{2}. \quad (24)$$

With this, we eliminate $\lambda(s, p_2)$ from Eqs. (21) and (23), and define $\phi = (s + p_2 - \lambda_f)/2$ to get $\dot{\phi} = -\phi^2$ and $\dot{s} = -2\phi s$. These equations are readily integrable from $t = 0$ to get

$$\phi(t) = \frac{\phi_i}{1 + \phi_i t} \quad \text{and} \quad s(t) = \frac{\lambda_i}{(1 + \phi_i t)^2}, \quad (25)$$

where we use $s(0) = \lambda_i$ and define the constant $\phi_i = \phi(0)$ yet to be determined. Equating $\phi(t_f) = (s(t_f) + p_2(t_f) - \lambda_f)/2$ allows us to solve

$$\phi_i = \frac{-(1 + \lambda_f t_f) + \sqrt{1 + 2\lambda_i t_f + \lambda_i \lambda_f t_f^2}}{2t_f + \lambda_f t_f^2}. \quad (26)$$

Finally, noting that $\lambda = s - \phi$, we obtain

$$\lambda(t) = \frac{\lambda_i - \phi_i(1 + \phi_i t)}{(1 + \phi_i t)^2}. \quad (27)$$

We readily identify Eqs. (26) and (27) as Eqs. (18) and (19) of [4]. Thus, from our optimal control Eqs. (17) and (18), we have analytically reproduced the optimal finite-time work-minimizing trajectory for a harmonic trap with variable stiffness. In Appendix A, we also analytically reproduce the optimal protocol for the variable trap center case $U(x, \lambda) = (x - \lambda)^2/2$ using our framework.

5 Numerically calculated optimal protocols

The harmonic potential problem is exceptional in that we can solve for its optimal protocol analytically. For the vast majority of time-varying potentials, the differential Eqs. (17) with constraint (20) do not admit analytic solutions, but can be solved numerically. In this section, we briefly sketch our numerical scheme to solve Eqs. (17) and (18), and we demonstrate our approach for two classes of quartic potential problems that do not admit analytic solutions: changing the stiffness of a quartic trap, and applying a linear bias to a double-well potential.

We compare the form and performance of these optimal protocols to three other protocols: naive, fast, and slow. The naive protocol interpolates the starting and ending parameters linearly in time $\lambda(t) = \lambda_i + (t/t_f)(\lambda_f - \lambda_i)$, and generally is not optimal in any regime. The fast protocol, also known as the short-time efficient protocol (STEP) as developed in [27], is optimal for small- t_f limit, and involves a step to an intermediate value λ^{STEP} for the duration of the protocol. The slow protocol first derived in [16], also known as the near-equilibrium protocol, is optimal for large t_f , and is obtained by considering the thermodynamic

geometry of protocol parameter space induced by the friction tensor $\xi(\lambda)$, from the linear response of excess work from changes in $\lambda(t)$. With this induced thermodynamic geometry, the slow protocol is a geodesic of ξ given by $\dot{\lambda}(t) \propto \xi(\lambda(t))^{-1/2}$, with $\lambda(0) = \lambda_i$ and $\lambda(t_f) = \lambda_f$. In Appendix sections B.1.4 and B.1.3, we review the slow and fast protocols in further detail, and show how we numerically produce them for our numerical study.

We first give a brief description of our method to numerically calculate optimal protocols, and then present our results for the variable-stiffness quartic trap and linearly biased double-well examples.

5.1 Brief description of numerical scheme to obtain optimal protocols

Here we briefly describe our discretization and integration scheme, referring the reader to Appendix B for details. Our lattice-discretization of space and time and approximated Fokker-Planck dynamics largely follow [48]. Just as taking the continuous limit from a discrete-state master equation yields Fokker-Planck dynamics, by discretizing our configuration space onto a lattice, Fokker-Planck dynamics can be approximated by a master equation over lattice states [49]. Here, we approximate the configuration space by a grid of d points with spacing Δx and reflecting boundaries at $x_b = \pm(d-1)\Delta x/2$, akin to the time-dependent Fokker-Planck discretization described in [48]. Our optimal control Eqs. (17) and (18) become the ordinary differential Eqs. (9) and (10), coupled by (11). Time is discretized to N time steps, with either constant or variable timesteps.

Because the transition rate matrix \mathcal{L}_λ has non-positive eigenvalues [50, 53], it is numerically unstable to integrate $\boldsymbol{\pi}$ forward in time, as any amount of numerical noise becomes exponentially amplified. Rather, we adopt a Forward-Backward sweep method [54, 32], where approximate solutions for $\boldsymbol{\rho}^{(k)}(t)$ and $\boldsymbol{\pi}^{(k)}(t)$ are updated iteratively through first obtaining $\boldsymbol{\rho}^{(k+1)}$ by solving (9) and (11) forwards in time starting with $\boldsymbol{\rho}(0) = \boldsymbol{\rho}_{i,\text{eq}}$, keeping $\boldsymbol{\pi}(t) = \boldsymbol{\pi}^{(k)}(t)$ fixed; and then obtaining $\boldsymbol{\pi}^{(k+1)}$ by solving (10) and (11) backwards in time starting with $\boldsymbol{\pi}(t_f) = \mathbf{0}$, keeping $\boldsymbol{\rho}(t) = \boldsymbol{\rho}^{(k+1)}(t)$ fixed. These forward and backward sweeps are iterated until numerical convergence of $\boldsymbol{\rho}^*(t), \boldsymbol{\pi}^*(t)$, which then is passed to (11) to obtain the optimal protocol $\lambda^*(t)$. More exact details of our numerical scheme may be found in Appendix B.

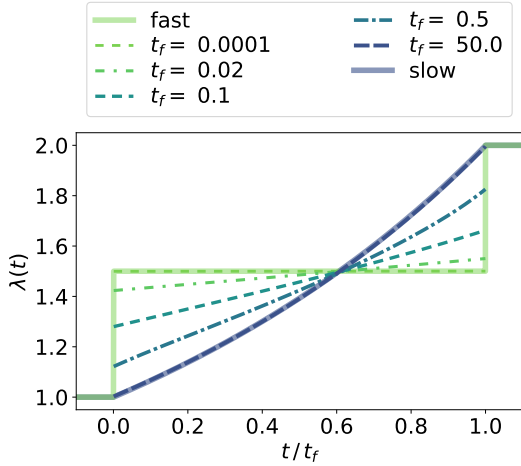
To measure the performance of each protocol $\lambda(t)$, we consider the excess work $W_{\text{ex}}[\lambda(t)] = W[\lambda(t)] - \Delta F$, where $\Delta F = \log(Z_f) - \log(Z_i)$ is the free energy difference between initial and final equilibrium states, with $Z_\lambda = \int dx \exp(-U_\lambda(x))$ being the partition function. By the Second Law of Thermodynamics, $W_{\text{ex}} > 0$, and approaches 0 in the quasistatic $t_f \rightarrow \infty$ limit. Appendix B.2 specifies how we numerically compute W_{ex} for a given protocol.

5.2 Quartic trap with variable stiffness

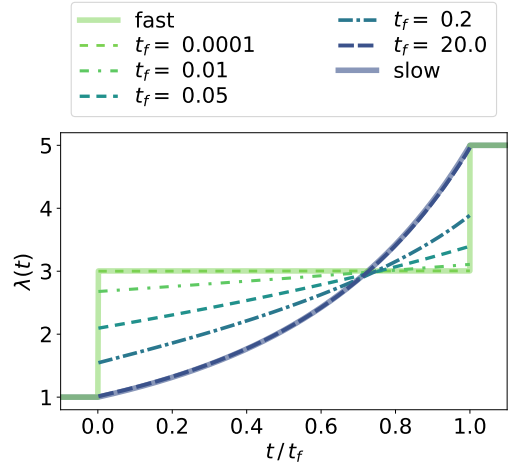
First, we consider the quartic analog of the variable stiffness harmonic oscillator, with the potential given as

$$U_\lambda(x) = \lambda \frac{x^4}{4}. \quad (28)$$

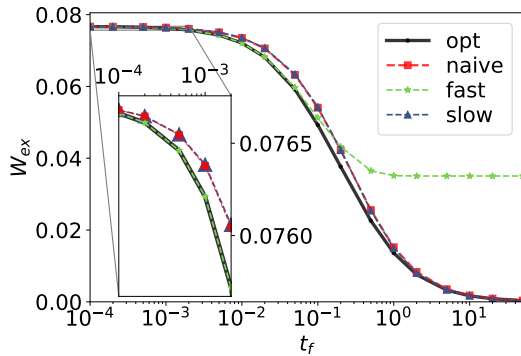
Figures 1a and 1b illustrate the numerically obtained optimal protocols for variable values of protocol time t_f , for $\lambda_i = 1, \lambda_f = 2$; and $\lambda_i = 1, \lambda_f = 5$ respectively. We see that the optimal protocols for the variable stiffness quartic trap problem are qualitatively similar to the optimal protocols for the variable stiffness harmonic trap in Section 4 (derived and illustrated in [4]). For both problems, optimal protocols are continuous and monotonic with positive curvature for times $t \in (0, t_f)$, and have discontinuous jumps at $t = 0$ and $t = t_f$.



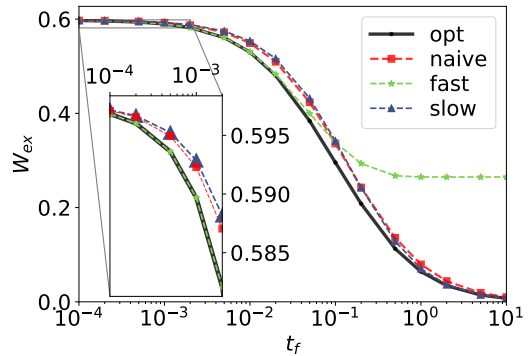
(a) Optimal protocol, $\lambda_i = 1, \lambda_f = 2$



(b) Optimal protocol, $\lambda_i = 1, \lambda_f = 5$



(c) Performance, $\lambda_i = 1, \lambda_f = 2$



(d) Performance, $\lambda_i = 1, \lambda_f = 2$

Figure 1: Form and performance of numerically produced optimal protocols for quartic trap with variable stiffness $U_\lambda(x) = \lambda x^4/4$ with $\lambda_i = 1, \lambda_f = 2$ on the left column, and $\lambda_i = 1, \lambda_f = 5$ on the right column. (a, b) illustrate optimal protocols for the trap stiffness, across various finite protocol duration values t_f . We see that for short times $t_f \ll 1$, the optimal protocol asymptotes to the fast protocol as given in [27], whereas for long times $t_f \gg 1$, the optimal protocol asymptotes to the slow protocol as given in [16]. We observe discontinuous jumps at $t = 0$ and $t = t_f$ in our numerically calculated optimal protocols, which is often the case for optimal protocols [4, 45, 5]. (c) and (d) compare the protocol performance W_{ex} among the numerically calculated optimal protocol, the fast protocol, the slow protocol, and the naive protocol. We see that the optimal protocol outperforms all other protocols, with the fast and slow protocols asymptoting in performance to the optimal protocol in their respective small- and large- t_f limits. The form and performance of these optimal protocols are qualitatively similar to those for the harmonic oscillator control case [4], which we have illustrated in Figure A.1.

Also plotted are the fast [27] and slow [16] protocols, which have been derived to be optimal for the small- and large- t_f limits, respectively. We see that the numerically solved optimal protocol asymptotes to these protocols in the respective t_f limits.

Figures 1c and 1d illustrate the excess work W_{ex} of various protocols across different time-scales t_f . We see that the optimal protocol outperforms all three of the naive, fast, and slow protocols. The performance of the fast protocol converges to the optimal protocol performance for short time-scales $t_f \ll 1$. Likewise, the performance of the slow protocol converges to the optimal protocol performance for long time-scales $t_f \gg 1$. This is expected, and is consistent with how the optimal protocol asymptotes to the fast and slow protocols in the respective time-scales.

5.3 Linearly biased double-well

Here we consider the double-well potential with wells at $x = \pm 1$ with an external linear bias

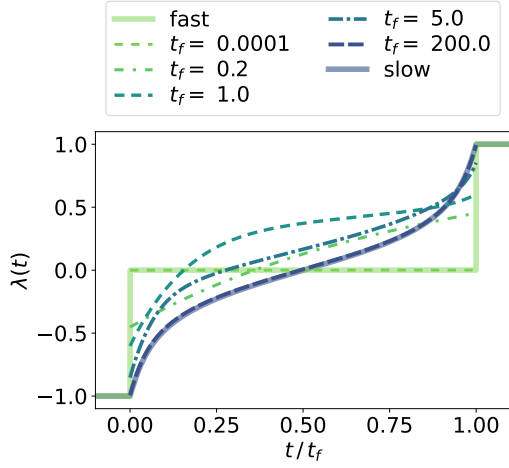
$$U_\lambda(x) = E_0 \frac{(x^2 - 1)^2}{4} - \lambda E_0 x. \quad (29)$$

Here, E_0 sets the energy scale of the ground and external potentials, with a barrier height of $E_0/4$ between the two wells at $\lambda = 0$. This potential is commonly used in the study of bit erasure [7, 8], but here we allow only limited control in the form of a linear bias. We note that this problem is qualitatively similar to the [24], where a harmonic pulling potential with variable center is applied to a potential with two local minima separated by a barrier. We consider $\lambda_i = -1$ and $\lambda_f = 1$, while varying E_0 and t_f . Setting the parameter value $\lambda = -1$ biases the potential to the left well, which sufficiently raises the right well above the barrier height and shifts the left well minimum from $x_{\text{well}} = -1$ to -1.32472 . Setting $\lambda = 1$ gives a symmetric bias to the right well.

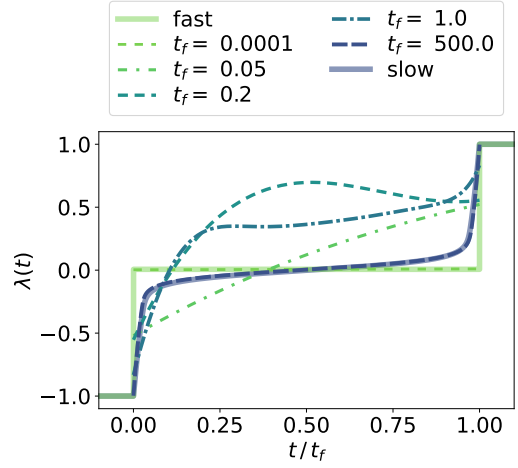
Figures 2a and 2b illustrate optimal protocols for $E_0 = 4$ and $E_0 = 16$, which correspond to inter-well barrier heights of $1 k_B T$ and $4 k_B T$ respectively. Just as before, the optimal protocol asymptotes to the fast and slow protocols in the small- and large- t_f limits. We note here that the optimal protocols obtained for various values of E_0 and t_f have intriguing properties. First of all, both the fast and slow protocols are symmetric under inversion $(\lambda(t), t) \rightarrow (-\lambda(t), t_f - t)$, which arises from the symmetry $U_\lambda(x) = U_{-\lambda}(-x)$ with $\lambda_f = -\lambda_i$, and the construction of these protocols. We see though that the optimal protocol obtained by solving (17) and (18) do not follow this symmetry for intermediate values of timescale t_f . This discovery of barrier crossing optimal protocols breaking symmetry was first made in [28]. At first this symmetry-breaking may seem counter-intuitive, but this can be understood by noting that λ_i and λ_f play completely different roles in our optimal control problem: λ_i specifies the initial condition $\rho(x, 0)$, while λ_f specifies $U_f(x)$ in the cost function.

Furthermore, not only do we find non-symmetric protocols, we discover that for $E_0 = 16$, the optimal protocol $\lambda(t)$ is non monotonic at certain intermediate timescales $t_f \sim 0.2$. This result is surprising, given that the underlying stochastic system (12) is overdamped — it has no momentum degrees of freedom that could incentivize overshoots. To our knowledge, no optimal or approximately-optimal protocols for a single parameter λ have been reported to exhibit this sort of non-monotonic behavior. In this regime, the optimal protocol cannot be interpreted as a geodesic for an underlying thermodynamic metric, as the latter can only produce monotonic protocols.

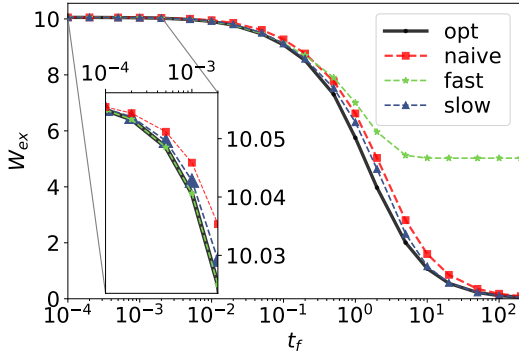
To explain this overshoot, we consider the mean position of the probability density under the optimal protocol $\langle x \rangle = \int \rho(x, t) x dx$ as a function time t . This is shown in Figures 3a and 3b, where we see $\langle x \rangle$



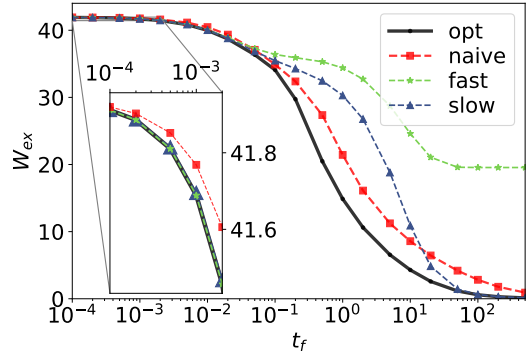
(a) Optimal protocol, $\lambda_i = -1, \lambda_f = 1, E_0 = 4$



(b) Optimal protocol, $\lambda_i = -1, \lambda_f = 1, E_0 = 16$

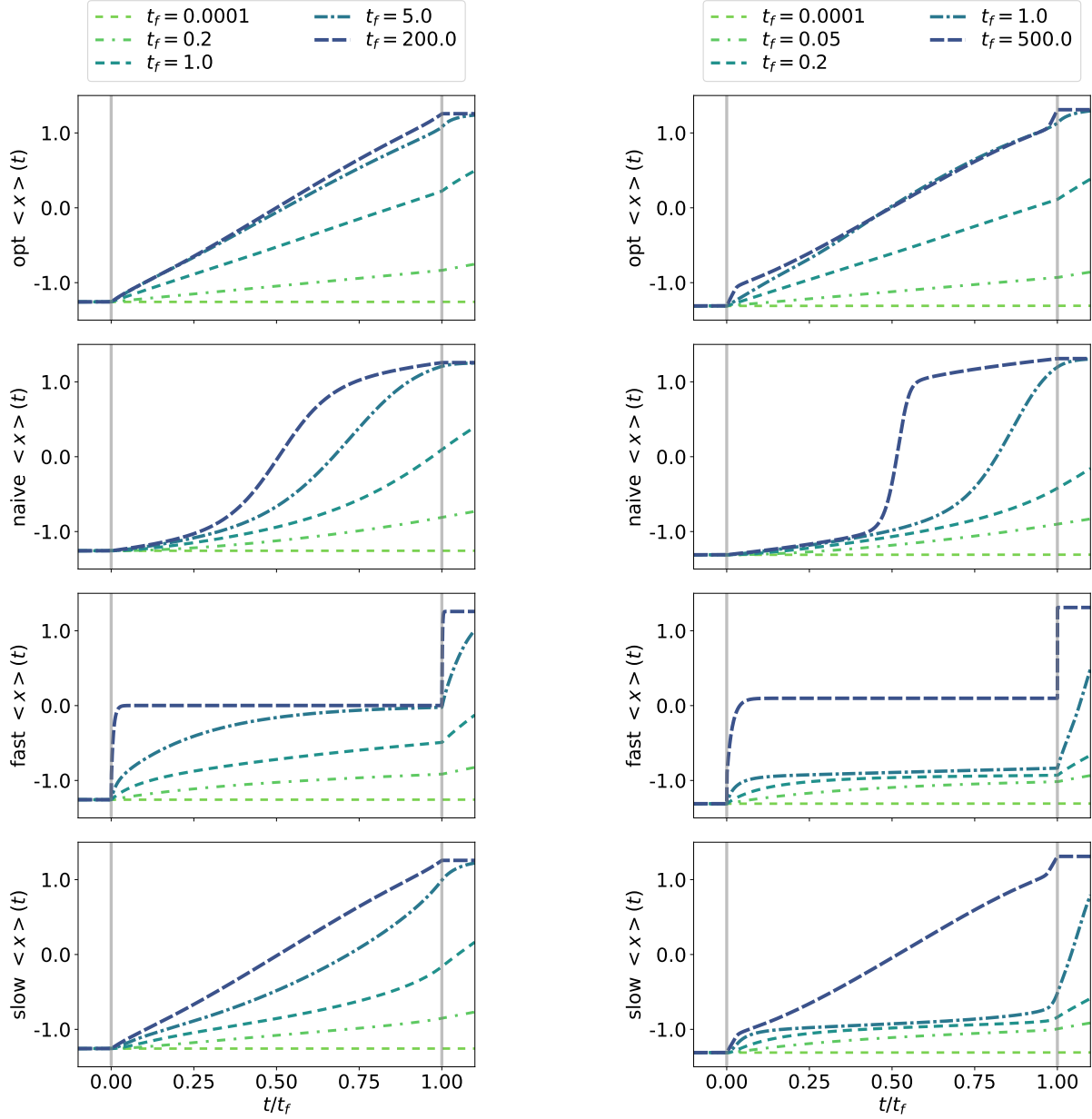


(c) Performance, $\lambda_i = -1, \lambda_f = 1, E_0 = 4$



(d) Performance, $\lambda_i = -1, \lambda_f = 1, E_0 = 16$

Figure 2: Numerically solved optimal protocols for the linearly biased double-well potential $U_\lambda(x) = E_0((x^2 - 1)^2/4 - \lambda x)$, $\lambda_i = -1$ and $\lambda_f = 1$; with $E_0 = 4$ in the left column, $E_0 = 16$ in the right. (a, b) illustrate the optimal protocols for the linear bias value, across various finite protocol duration values t_f . As with the quartic case in Fig. 1, here for short times $t_f \ll 1$ and long times $t_f \gg 1$, the optimal protocol asymptotes to the fast and slow protocols respectively. Unlike the slow and fast protocols, for intermediate values of t_f the optimal protocols are not symmetric in $(t, \lambda) \rightarrow (-t, -\lambda)$. For $E_0 = 16$, we observe surprising non-monotonic protocols for $t_f \sim 0.2$. (c, d) depict the protocol performance W_{ex} between the numerically calculated optimal protocol and other protocols. Like in the quartic case, we see that the optimal protocol outperforms all other protocols, with the fast and slow protocols asymptoting in performance to the optimal protocol in their respective small- and large- t_f limits. For $E_0 = 16$, the optimal protocol vastly outperforms the other protocols for $t_f \sim 2$.



(a) Distribution mean, $\lambda_i = -1, \lambda_f = 1, E_0 = 4$

(b) Distribution mean, $\lambda_i = -1, \lambda_f = 1, E_0 = 16$

Figure 3: The evolution of the expected mean $\langle x \rangle(t)$ for the linearly biased double-well problem $U_\lambda(x) = E_0((x^2 - 1)^2/4 - \lambda x)$, across various protocol duration values t_f . Here, $\lambda_i = -1$ and $\lambda_f = 1$, with (a) $E_0 = 4$, and (b) $E_0 = 16$. The first row depicts the optimal protocol, the second the naive protocol, the third the fast protocol, and the fourth the slow protocol. For the optimal protocol, $\langle x \rangle(t)$ increases monotonically with near-constant velocity, which we argue is a generic property of limited-control optimal controls. Compared to the optimal protocol, the naive, fast, and slow protocols evolve the mean $\langle x \rangle(t)$ with much more variable velocity. The deviation from constant-velocity roughly corresponds to larger W_{ex} values, as depicted in Figs. 2c and 2d.

increases at a nearly constant rate under the optimal protocol. This may be interpreted as the limited-control optimal protocol allowing barrier-crossing to occur at an approximately constant velocity. In Appendix C, we draw from optimal transport theory to show that when full control over the potential is allowed, $\langle x \rangle$ always maintains a constant speed throughout the optimal trajectory. This suggests that insofar as a limited-control optimal protocol should approximate the full-control optimal protocol, it drives the mean of the probability distribution to travel with near-constant velocity, even if requiring an overshoot as is the case for the $E_0 \sim 16, t_f \sim 0.2$ regime.

Figures 2c and 2d illustrate the performance of these protocols. Just as we found for the harmonic potential, the OCT protocol outperforms all three other considered protocols, with performance of fast and slow protocols approaching the optimal protocol performance in their respective t_f limits. We see that for barrier height $E_0 = 16$, the optimal protocol vastly outperforms all other protocols at intermediate t_f values. For instance, at $t_f = 2$ the optimal protocol gives $W_{\text{ex}} = 10.61$, which is significantly smaller than the naive protocol $W_{\text{ex}} = 16.12$ and slow protocol $W_{\text{ex}} = 26.77$ values. This shows the existence of truly far from equilibrium regimes, for which protocols derived assuming either fast or near-equilibrium approximations deviate significantly from the true, fully non-equilibrium optimal protocol, in both form and performance.

6 Discussion

It is typically the case in experimental and engineering contexts that only a finite set of degrees of freedom of a system is controllable. We have shown that the problem of finding work-minimizing optimal protocols is naturally framable as an optimal control theory (OCT) problem. Using tools and techniques from OCT, we have devised a method to derive optimal protocols in the case where there is only limited control of the form of the system's potential. Our framework allows us to reproduce known analytic results for the control of a harmonic oscillator, as well as to efficiently calculate optimal protocols numerically for a large class of limited-control potentials.

Previous work on dissipation-minimizing optimal protocols revealed thermodynamic geometry on protocol parameter space through the friction tensor [16, 53], and on probability density space through the L^2 -Wasserstein metric [55, 13, 14, 15]. We have found that the protocol optimization problem has a deep Hamiltonian structure, typical of OCT problems [31]. It is interesting to ponder what insights may be gleaned from the study of optimal protocols for non-equilibrium processes when both Riemmanian and symplectic structures are considered together.

It is straightforward to generalize our results configuration and parameter spaces that are multi-dimensional, which suggests a number of natural extensions. First, by allowing time-varying control of temperature $\beta^{-1} = k_B T$ and asserting time-periodicity for the protocol, we can construct optimal finite-time heat engines arbitrarily far from equilibrium, building off of [10, 55]. Cyclical protocols may also be considered for when the state space and/or configuration space are non-Euclidean manifolds [17]; e.g., for the external control of rotary motor proteins like F_oF_1 [56]. Finally, it would be intriguing to extend our framework to the study of underdamped systems where both position and velocity degrees of freedom (x, v) make up the configuration space [6, 57], as because the kinetic term of the underlying Klein-Kramers equation cannot be controlled, control is intrinsically limited to just the spatial degrees of freedom.

When the configuration space has many degrees of freedom, the curse of dimensionality kicks in, where the memory required to store the probability distribution is exponential in the number of dimensions of the configuration space [58]. In this case, it may be more computationally tractable to sample individual

stochastic trajectories to compute the friction tensor [16, 59] or gradients of the protocol [28] in order to calculate optimal protocols. It will be of interest to study the effectiveness of configuration space dimensionality reduction techniques (e.g., density functional theory [60], Zwanzig-Mori projection operators [49]) to make the calculation of optimal protocols through our framework computationally tractable for high dimensional configuration spaces.

We have shown that optimal control theory is a natural and powerful framework for the design and study of thermodynamically optimal protocols. In the spirit of [61], it is our hope that through considering the optimal control of non-equilibrium probability densities considered here and elsewhere [34, 36, 33], we may better understand how it is that biological systems, which operate far from equilibrium, function efficiently across vastly different length- and time-scales.

7 Acknowledgements

The authors would like to thank Benjamin Kuznets-Speck and David Limmer for insightful conversations, and Adam Frim for helpful manuscript comments. This research used the Savio computational cluster resource provided by the Berkeley Research Computing program at the University of California, Berkeley (supported by the UC Berkeley Chancellor, Vice Chancellor for Research, and Chief Information Officer). AZ was supported by the Department of Defense (DoD) through the National Defense Science & Engineering Graduate (NDSEG) Fellowship Program. This work was supported in part by the U. S. Army Research Laboratory and the U. S. Army Research Office under Contract No. W911NF-20-1-0151.

References

- [1] Udo Seifert. “Stochastic thermodynamics, fluctuation theorems and molecular machines”. In: *Reports on progress in physics* 75.12 (2012), p. 126001.
- [2] Christopher Jarzynski, Wolfram Just, and Rainer Klages. *Nonequilibrium statistical physics of small systems*. Wiley-VCH Verlag GmbH & Company KGaA, 2013.
- [3] Sergio Ciliberto. “Experiments in stochastic thermodynamics: Short history and perspectives”. In: *Physical Review X* 7.2 (2017), p. 021051.
- [4] Tim Schmiedl and Udo Seifert. “Optimal finite-time processes in stochastic thermodynamics”. In: *Physical review letters* 98.10 (2007), p. 108301.
- [5] Steven Blaber and David A Sivak. “Skewed thermodynamic geometry and optimal free energy estimation”. In: *The Journal of Chemical Physics* 153.24 (2020), p. 244119.
- [6] Alex Gomez-Marin, Tim Schmiedl, and Udo Seifert. “Optimal protocols for minimal work processes in underdamped stochastic thermodynamics”. In: *The Journal of chemical physics* 129.2 (2008), p. 024114.
- [7] Karel Proesmans, Jannik Ehrich, and John Bechhoefer. “Optimal finite-time bit erasure under full control”. In: *Physical Review E* 102.3 (2020), p. 032105.
- [8] Patrick R Zulkowski and Michael R DeWeese. “Optimal finite-time erasure of a classical bit”. In: *Physical Review E* 89.5 (2014), p. 052140.
- [9] Valentin Blickle and Clemens Bechinger. “Realization of a micrometre-sized stochastic heat engine”. In: *Nature Physics* 8.2 (2012), pp. 143–146.

- [10] Adam G Frim and Michael R DeWeese. “Optimal finite-time Brownian Carnot engine”. In: *arXiv preprint arXiv:2107.05673* (2021).
- [11] Adam G Frim and Michael R DeWeese. “A geometric bound on the efficiency of irreversible thermodynamic cycles”. In: *arXiv preprint arXiv:2112.10797* (2021).
- [12] Erik Aurell, Carlos Mejía-Monasterio, and Paolo Muratore-Ginanneschi. “Optimal protocols and optimal transport in stochastic thermodynamics”. In: *Physical review letters* 106.25 (2011), p. 250601.
- [13] Andreas Dechant and Yohei Sakurai. “Thermodynamic interpretation of Wasserstein distance”. In: *arXiv preprint arXiv:1912.08405* (2019).
- [14] Muka Nakazato and Sosuke Ito. “Geometrical aspects of entropy production in stochastic thermodynamics based on Wasserstein distance”. In: *arXiv preprint arXiv:2103.00503* (2021).
- [15] Yongxin Chen, Tryphon T Georgiou, and Allen Tannenbaum. “Stochastic control and nonequilibrium thermodynamics: Fundamental limits”. In: *IEEE transactions on automatic control* 65.7 (2019), pp. 2979–2991.
- [16] David A Sivak and Gavin E Crooks. “Thermodynamic metrics and optimal paths”. In: *Physical review letters* 108.19 (2012), p. 190602.
- [17] Adam G Frim et al. “Engineered swift equilibration for arbitrary geometries”. In: *Physical Review E* 103.3 (2021), p. L030102.
- [18] Efe Ilker et al. “Counterdiabatic control of biophysical processes”. In: *arXiv preprint arXiv:2106.07130* (2021).
- [19] Ignacio A Martínez et al. “Engineered swift equilibration of a Brownian particle”. In: *Nature physics* 12.9 (2016), pp. 843–846.
- [20] Cédric Villani. *Optimal transport: old and new*. Vol. 338. Springer, 2009.
- [21] Shriram Chennakesavalu and Grant M. Rotskoff. *Unifying thermodynamic geometries*. 2022. arXiv: 2205.01205 [cond-mat.stat-mech].
- [22] Holger Then and Andreas Engel. “Computing the optimal protocol for finite-time processes in stochastic thermodynamics”. In: *Physical Review E* 77.4 (2008), p. 041105.
- [23] Carlos A Plata et al. “Optimal work in a harmonic trap with bounded stiffness”. In: *Physical Review E* 99.1 (2019), p. 012140.
- [24] David A Sivak and Gavin E Crooks. “Thermodynamic geometry of minimum-dissipation driven barrier crossing”. In: *Physical Review E* 94.5 (2016), p. 052106.
- [25] Patrick R Zulkowski et al. “Geometry of thermodynamic control”. In: *Physical Review E* 86.4 (2012), p. 041148.
- [26] Sebastian Deffner and Marcus VS Bonança. “Thermodynamic control—An old paradigm with new applications”. In: *EPL (Europhysics Letters)* 131.2 (2020), p. 20001.
- [27] Steven Blaber, Miranda D Louwerse, and David A Sivak. “Steps Minimize Dissipation in Rapidly Driven Stochastic Systems”. In: *arXiv preprint arXiv:2105.04691* (2021).
- [28] Megan C Engel, Jamie A Smith, and Michael P Brenner. “Optimal control of nonequilibrium systems through automatic differentiation”. In: *arXiv preprint arXiv:2201.00098* (2022).

- [29] Jiawei Yan, Hugo Touchette, Grant M Rotskoff, et al. “Learning nonequilibrium control forces to characterize dynamical phase transitions”. In: *Physical Review E* 105.2 (2022), p. 024115.
- [30] Avishek Das, Benjamin Kuznets-Speck, and David T Limmer. “Direct evaluation of rare events in active matter from variational path sampling”. In: *Physical Review Letters* 128.2 (2022), p. 028005.
- [31] Daniel Liberzon. “Calculus of variations and optimal control theory”. In: *Calculus of Variations and Optimal Control Theory*. Princeton university press, 2011.
- [32] Suzanne Lenhart and John T Workman. *Optimal control applied to biological models*. Chapman and Hall/CRC, 2007.
- [33] Kaivlaya Bakshi and Evangelos A Theodorou. “Open-loop Deterministic Density Control of Marked Jump Diffusions”. In: *arXiv preprint arXiv:2009.07154* (2020).
- [34] Mario Annunziato and Alfio Borzi. “A Fokker–Planck control framework for multidimensional stochastic processes”. In: *Journal of Computational and Applied Mathematics* 237.1 (2013), pp. 487–507.
- [35] Hector O Fattorini, Hector O Fattorini, et al. *Infinite dimensional optimization and control theory*. Vol. 54. Cambridge University Press, 1999.
- [36] Aaron Palmer and Dejan Milutinović. “A hamiltonian approach using partial differential equations for open-loop stochastic optimal control”. In: *Proceedings of the 2011 American Control Conference*. IEEE. 2011, pp. 2056–2061.
- [37] Ethan N Evans et al. “Spatio-Temporal Differential Dynamic Programming for Control of Fields”. In: *arXiv preprint arXiv:2104.04044* (2021).
- [38] Evangelos A Theodorou and Emmanuel Todorov. “Stochastic optimal control for nonlinear Markov jump diffusion processes”. In: *2012 American Control Conference (ACC)*. IEEE. 2012, pp. 1633–1639.
- [39] Arthur Fleig and Roberto Guglielmi. “Optimal control of the Fokker–Planck equation with space-dependent controls”. In: *Journal of Optimization Theory and Applications* 174.2 (2017), pp. 408–427.
- [40] Mario Annunziato and Alfio Borzi. “Optimal control of probability density functions of stochastic processes”. In: *Mathematical Modelling and Analysis* 15.4 (2010), pp. 393–407.
- [41] Mihai Popescu et al. “Existence and Uniqueness of the Optimal Control in Hilbert Spaces for a Class of Linear Systems”. In: *Intelligent Information Management* 2.02 (2010), p. 134.
- [42] Vladimir Y Chernyak et al. “Stochastic optimal control as non-equilibrium statistical mechanics: Calculus of variations over density and current”. In: *Journal of Physics A: Mathematical and Theoretical* 47.2 (2013), p. 022001.
- [43] Jascha Sohl-Dickstein, Peter Battaglino, and Michael R DeWeese. “Minimum probability flow learning”. In: *arXiv preprint arXiv:0906.4779* (2009).
- [44] Stefano Bo, Soon Hoe Lim, and Ralf Eichhorn. “Functionals in stochastic thermodynamics: how to interpret stochastic integrals”. In: *Journal of Statistical Mechanics: Theory and Experiment* 2019.8 (2019), p. 084005.
- [45] Erik Aurell, Carlos Meji’a-Monasterio, and Paolo Muratore-Ginanneschi. “Boundary layers in stochastic thermodynamics”. In: *Physical Review E* 85.2 (2012), p. 020103.
- [46] John Robert Taylor. *Classical mechanics*. 531 TAY. 2005.
- [47] Jorge José and Eugene Saletan. *Classical dynamics: a contemporary approach*. 2000.

- [48] Viktor Holubec, Klaus Kroy, and Stefano Steffenoni. “Physically consistent numerical solver for time-dependent Fokker-Planck equations”. In: *Physical Review E* 99.3 (2019), p. 032117.
- [49] Robert Zwanzig. *Nonequilibrium statistical mechanics*. Oxford university press, 2001.
- [50] Hannes Risken. “Fokker-planck equation”. In: *The Fokker-Planck Equation*. Springer, 1996, pp. 63–95.
- [51] Carlos J Bustamante et al. “Optical tweezers in single-molecule biophysics”. In: *Nature Reviews Methods Primers* 1.1 (2021), pp. 1–29.
- [52] Gerhard Hummer and Attila Szabo. “Free energy reconstruction from nonequilibrium single-molecule pulling experiments”. In: *Proceedings of the National Academy of Sciences* 98.7 (2001), pp. 3658–3661.
- [53] Neha S Wadia, Ryan V Zarcone, and Michael R DeWeese. “Solution to the Fokker-Planck equation for slowly driven Brownian motion: Emergent geometry and a formula for the corresponding thermodynamic metric”. In: *Physical Review E* 105.3 (2022), p. 034130.
- [54] Michael McAsey, Libin Mou, and Weimin Han. “Convergence of the forward-backward sweep method in optimal control”. In: *Computational Optimization and Applications* 53.1 (2012), pp. 207–226.
- [55] Gentaro Watanabe and Yuki Minami. “Finite-time thermodynamics of fluctuations in microscopic heat engines”. In: *Physical Review Research* 4.1 (2022), p. L012008.
- [56] Joseph NE Lucero, Aliakbar Mehdizadeh, and David A Sivak. “Optimal control of rotary motors”. In: *Physical Review E* 99.1 (2019), p. 012119.
- [57] Paolo Muratore-Ginanneschi. “On extremals of the entropy production by ‘Langevin–Kramers’ dynamics”. In: *Journal of Statistical Mechanics: Theory and Experiment* 2014.5 (2014), P05013.
- [58] Hilbert J Kappen. “Path integrals and symmetry breaking for optimal control theory”. In: *Journal of statistical mechanics: theory and experiment* 2005.11 (2005), P11011.
- [59] Grant M Rotskoff and Gavin E Crooks. “Optimal control in nonequilibrium systems: Dynamic Riemannian geometry of the Ising model”. In: *Physical Review E* 92.6 (2015), p. 060102.
- [60] Michael te Vrugt, Hartmut Löwen, and Raphael Wittkowski. “Classical dynamical density functional theory: from fundamentals to applications”. In: *Advances in Physics* 69.2 (2020), pp. 121–247.
- [61] Ty NF Roach et al. “Application of finite-time and control thermodynamics to biological processes at multiple scales”. In: *Journal of Non-Equilibrium Thermodynamics* 43.3 (2018), pp. 193–210.

Appendix A Analytic optimal protocol for moving harmonic trap

Here, we reproduce the optimal protocol for a moving harmonic trap, with control potential

$$U_\lambda(x) = \frac{(x - \lambda)^2}{2} \quad (30)$$

starting at $\lambda_i = 0$ and ending at some $\lambda_f \neq 0$ in time t_f . Writing $U_\lambda(x) = U_0(x) + \lambda U_1(x) + U_c(\lambda)$, we identify $U_0(x) = x^2/2$, $U_1(x) = -x$, and $U_c(\lambda) = \lambda^2/2$. The initial equilibrium distribution is a Gaussian with mean μ centered at 0 with variance 1, and evolves as a Gaussian with a shifting mean given by

$$\dot{\mu} = \lambda - \mu, \quad (31)$$

obtained by plugging a Gaussian ρ of unit variance into Eq. (17).

Considering a truncated polynomial ansatz $\pi(x, t) = \sum_{k=0}^n p_k(t) x^k/k!$ for the conjugate momentum, Eq. (17) and the terminal condition $\pi(x, t_f) = 0$ lead to the survival of only the linear term $\pi(x, t) = p_1(t)x$, with dynamics

$$\dot{p}_1 = p_1 + \lambda_f - \lambda. \quad (32)$$

Finally, the constraint Eq. (20) gives us

$$\lambda[\rho, \pi] = \frac{\lambda_f + \mu + p_1}{2}. \quad (33)$$

Plugging this in to (31) and (32), we obtain

$$\begin{aligned} \dot{\mu} = \dot{p}_1 &= \frac{\lambda_f + p_1 - \mu}{2} \\ &= \frac{\lambda_f - \delta}{2} \end{aligned} \quad (34)$$

where we get the second line from seeing that because $\dot{\mu} = \dot{p}_1$, the difference $\delta = \mu(t) - p_1(t)$ is time-independent. Thus, we see that μ and p_1 change at a constant and equal rate. Given our boundary conditions $\mu(0) = 0$ and $p_1(t_f) = 0$, we have $\mu(t) = (\lambda_f - \delta)t/2$ and $p_1(t) = (\lambda_f - \delta)(t - t_f)/2$. Setting $\mu(t_f) - p_1(t_f) = \delta$, we get

$$\delta = \left(\frac{\lambda_f - \delta}{2} \right) t_f \quad (35)$$

which is easily solved as $\delta = \lambda_f t_f / (t_f + 2)$.

Thus, we have

$$\mu(t) = \frac{\lambda_f t}{t_f + 2} \quad (36)$$

$$p_1(t) = \frac{\lambda_f(t - t_f)}{t_f + 2} \quad (37)$$

which we plug into (33) to obtain

$$\lambda(t) = \frac{\lambda_f(t+1)}{t_f+2}, \quad (38)$$

and thus reproducing the optimal protocol in equation (9) of [1].

Appendix B Numerical Methods

Here, we discuss how we numerically obtain the optimal, naive, fast, and slow protocols. In general, our lattice-discretization and discretized Fokker-Planck dynamics follow [2].

We discretize our configuration space with a lattice of d points with spacing Δx with reflecting boundaries at $x_b = \pm(d-1)\Delta x/2$. The values of $\rho(x, t)$, $\pi(x, t)$, and $U(x, \lambda)$ are approximated by $\boldsymbol{\rho}(t)$, $\boldsymbol{\pi}(t)$, and $\mathbf{U}_\lambda(t)$, with $[\boldsymbol{\rho}(t)]^l = \rho(x(l), t)$, $[\boldsymbol{\pi}(t)]_l = \pi(x(l), t)$, and $[\mathbf{U}_\lambda]_l = U(x(l), \lambda)$, where $x(l) = (2l+1-d)\Delta x/2$, with $l = 1, 2, \dots, d$. The Fokker-Planck operator $\hat{\mathcal{L}}_\lambda$ is approximated then by the appropriate transition rate matrix \mathcal{L}_λ from (2), with $c_{ij} = D(\Delta x)^{-2}$ for all neighboring sites $|i-j|=1$, and $c_{ij} = 0$ for all else.

Time is discretized to $\{t_n \mid n = 0, 1, \dots, N; t_0 = 0, t_N = t_f\}$ with (not necessarily even) time steps $h_n = t_n - t_{n-1}$, and each protocol is given as $\{\lambda_n, \mid n = 1, \dots, N\}$, each λ_n defined between time points (t_{n-1}, t_n) .

We first describe how we obtain each of the protocols in B.1, and then how the excess work of each protocol W_{ex} is numerically computed in B.2, and finally our specific spatial and time discretization parameters (and corresponding computational performance) in B.3.

B.1 Numerical computation of optimal, naive, fast, and slow protocols

B.1.1 Optimal protocol

Given our spatial discretization, we must numerically solve the coupled differential equations

$$\dot{\boldsymbol{\rho}} = \mathcal{L}_\lambda \boldsymbol{\rho} \quad (39)$$

$$\dot{\boldsymbol{\pi}} = -\mathcal{L}_\lambda^T (\boldsymbol{\pi} + \mathbf{U}_\lambda - \mathbf{U}_f) \quad (40)$$

with mixed initial and final conditions $\boldsymbol{\rho}(0) = \boldsymbol{\rho}_i$, $\boldsymbol{\pi}(t_f) = \mathbf{0}$. The two equations are coupled together by the constraint equation

$$\left(\left[\frac{d\mathbf{U}_\lambda}{d\lambda} \right]^T \mathcal{L}_\lambda + (\boldsymbol{\pi} + \mathbf{U}_\lambda - \mathbf{U}_f)^T \frac{d\mathcal{L}_\lambda}{d\lambda} \right) \boldsymbol{\rho} = 0, \quad (41)$$

which may be numerically invertible through an iterative root-finding algorithm to obtain $\lambda(\boldsymbol{\rho}, \boldsymbol{\pi})$.

Generically, the Fokker-Planck operator (13), which is discretized as matrix \mathcal{L}_λ , has an unbounded spectrum of non-positive eigenvalues [3, 4]. This makes the differential equations stiff to numerically integrate. In particular, the numerical integration of $\boldsymbol{\pi}$ forwards in time is numerically unstable, as any finite amount of numerical noise becomes exponentially amplified. The same holds true for the numerical integration of $\boldsymbol{\rho}$ backwards in time.

To circumvent this problem, we use a modified version of the iterative Forward-Backward Sweep Method [5, 6] that explicitly avoids integrating $\boldsymbol{\pi}$ forward in time and $\boldsymbol{\rho}$ backward in time. Briefly, one starts with

a guess of the solution $\{\boldsymbol{\rho}^{(0)}(t), \boldsymbol{\pi}^{(0)}(t)\}$. At each iteration, our approximate solution $\{\boldsymbol{\rho}^{(k)}(t), \boldsymbol{\pi}^{(k)}(t)\}$ is updated through a forward and a backward sweep. In the forward sweep, $\boldsymbol{\rho}^{(k+1)}(t)$ is obtained by numerically integrating (39) forward in time, using $\boldsymbol{\pi}^{(k)}(t)$ to evaluate $\lambda(\boldsymbol{\rho}, \boldsymbol{\pi})$. Next, for the backward sweep, $\boldsymbol{\pi}^{(k+1)}(t)$ is obtained by numerically integrating (40) backward in time using the values of $\lambda(\boldsymbol{\rho}, \boldsymbol{\pi})$ from the forward sweep. Through enough iterations, the iterative solution $\{\boldsymbol{\rho}^{(k)}(t), \boldsymbol{\pi}^{(k)}(t)\}$ converges to a "fixed point" $\{\boldsymbol{\rho}^*(t), \boldsymbol{\pi}^*(t)\}$ that does not change under further iterations. This would be our solution to (39), (40), and (41), with $\{\lambda^*(t) = \lambda(\boldsymbol{\rho}^*(t), \boldsymbol{\pi}^*(t))\}$.

Corresponding to the time discretization, $\{\boldsymbol{\rho}(t), \boldsymbol{\pi}(t)\}$ is discretized to $\{(\boldsymbol{\rho}_n, \boldsymbol{\pi}_n) \mid n = 0, 1, \dots, N\}$. We note that due to the Hamiltonian nature of the continuous-time dynamics, we use an symplectic exponential integrator to preserve the underlying Hamiltonian structure [7, 8]. The forward sweep to obtain $\{\boldsymbol{\rho}_n^{(k+1)} \mid n = 0, 1, \dots, N\}$ consists of iteratively taking forward steps from t_n to t_{n+1} through

$$\boldsymbol{\rho}_{n+1}^{(k+1)}(\boldsymbol{\rho}_n^{(k+1)}, \boldsymbol{\pi}_{n+1}^{(k)}) = e^{h_{n+1}\mathcal{L}_\lambda} \boldsymbol{\rho}_n^{(k+1)} \Big|_{\lambda = \lambda(\boldsymbol{\rho}_n^{(k+1)}, \boldsymbol{\pi}_{n+1}^{(k)})} \quad (42)$$

starting with the initial condition $\boldsymbol{\rho}_0^{(k+1)} = \boldsymbol{\rho}_i$. At each step, $\lambda(\boldsymbol{\rho}_n^{(k+1)}, \boldsymbol{\pi}_{n+1}^{(k)})$ that satisfies the constraint equation.

The backward sweep to obtain $\{\boldsymbol{\pi}_n^{(k+1)} \mid n = 0, 1, \dots, N\}$ is done similarly, by iteratively taking backward steps from t_{n+1} to t_n through

$$\boldsymbol{\pi}_n^{(k+1)}(\boldsymbol{\rho}_n^{(k+1)}, \boldsymbol{\pi}_{n+1}^{(k+1)}) = e^{h_{n+1}\mathcal{L}_\lambda^T} \boldsymbol{\pi}_{n+1}^{(k+1)} + (e^{h_{n+1}\mathcal{L}_\lambda^T} - \mathbb{1})(\mathbf{U}_\lambda - \mathbf{U}_f) \Big|_{\lambda = \lambda(\boldsymbol{\rho}_n^{(k+1)}, \boldsymbol{\pi}_{n+1}^{(k+1)})}. \quad (43)$$

starting with the final condition $\boldsymbol{\pi}_N^{(k+1)} = \mathbf{0}$ and descending to $n = 0$. Here $\mathbb{1}$ denotes the d -dimensional identity matrix. Note here, we use the λ values obtained in the forward sweep.

During each forward sweep, $\lambda(\boldsymbol{\rho}_n^{(k+1)}, \boldsymbol{\pi}_{n+1}^{(k+1)})$ is calculated numerically. Due to the discretization of time, the constraint equation is slightly different. We first note that Eqs. (42) and (43) correspond to the following discrete Lagrangian

$$L[\{(\boldsymbol{\rho}_n, \boldsymbol{\pi}_n)\}] = \sum_{n=0}^{N-1} \left[-(\mathbf{U}_\lambda - \mathbf{U}_f)^T (e^{h_{n+1}\mathcal{L}_\lambda} - \mathbb{1}) \boldsymbol{\rho}_n + \boldsymbol{\pi}_{n+1}^T (\boldsymbol{\rho}_{n+1} - e^{h_{n+1}\mathcal{L}_\lambda} \boldsymbol{\rho}_n) \right]_{\lambda = \lambda(\boldsymbol{\rho}_n, \boldsymbol{\pi}_{n+1})}, \quad (44)$$

as taking $\partial L / \partial \boldsymbol{\pi}_n = 0$ and $\partial L / \partial \boldsymbol{\rho}_n = 0$ reproduce them. Taking $\partial L / \partial \lambda = 0$ for each $\lambda(\boldsymbol{\rho}_n, \boldsymbol{\pi}_{n+1})$ gives the constraint equation

$$\left[\left(\frac{d\mathbf{U}_\lambda}{d\lambda} \right)^T (e^{h_{n+1}\mathcal{L}_\lambda} - \mathbb{1}) + (\boldsymbol{\pi}_{n+1} + \mathbf{U}_\lambda - \mathbf{U}_f)^T \left(\frac{\partial (e^{h_{n+1}\mathcal{L}_\lambda})}{\partial \lambda} \right) \right] \boldsymbol{\rho}_n \Big|_{\lambda = \lambda(\boldsymbol{\rho}_n, \boldsymbol{\pi}_{n+1})} = 0 \quad (45)$$

where the partial derivative of the matrix exponential may be numerically computed through [9]. It may be seen that in the $h_{n+1} \rightarrow 0$ limit, this equation is equivalent to (41). For each of the steps taken in a forward sweep, the protocol value $\lambda(\boldsymbol{\rho}_n, \boldsymbol{\pi}_{n+1})$ is numerically calculated to satisfy (45) through a root-finding algorithm.

To start our forward-backward sweep algorithm, we use the slow protocol $\{\lambda_n^{\text{slow}}\}$ described in B.1.4, to get $\{\boldsymbol{\pi}_n^{(0)}\}$ through

$$\begin{aligned}\boldsymbol{\pi}_{N+1}^{(0)} &= \mathbf{0} \\ \boldsymbol{\pi}_n^{(0)} &= e^{h_{n+1}\mathcal{L}_\lambda^T} \boldsymbol{\pi}_{n+1}^{(0)} + (e^{h_{n+1}\mathcal{L}_\lambda^T} - \mathbb{1})(\mathbf{U}_\lambda - \mathbf{U}_f)|_{\lambda=\lambda_{n+1}^{\text{slow}}}.\end{aligned}$$

It is this $\{\boldsymbol{\pi}_n^{(0)}\}$ that we use as the initial condition to start our first forward sweep. (Note, the value of initial $\{\boldsymbol{\rho}_n^{(0)}\}$ does not matter, as it is not used at all in the first forward-backward sweep iteration.)

Forward and backward sweeps are iteratively done until numerical convergence, which we chose to be when the root-mean-squared difference of $\{\lambda_n^{(k)}\}$ and $\{\lambda_n^{(k+1)}\}$ between adjacent iterations is less than 10^{-8} . Interestingly, the number of forward-backward sweep iterations until convergence varies as a function of t_f , increasing for larger values of t_f , which we discuss in B.3

B.1.2 Naive protocol

The naive protocol is a linear interpolation between λ_i and λ_f , i.e. $\lambda^{\text{naive}}(t) = \lambda_i + (t/t_f)(\lambda_f - \lambda_i)$. The discretized version is given as

$$\left\{ \lambda_n^{\text{naive}} = \lambda_i + \frac{t_n + t_{n-1}}{2t_f}(\lambda_f - \lambda_i) \mid n = 1, \dots, N \right\}. \quad (46)$$

B.1.3 Fast protocol

It was shown in [10] that for small time-scales $t_f \ll 1$, the optimal protocol is given by a step at intermediate times

$$\lambda(t) = \begin{cases} \lambda_i & \text{for } t = 0 \\ \lambda^{\text{STEP}} & \text{for } t \in (0, t_f) \\ \lambda_f & \text{for } t = t_f \end{cases}$$

with a single optimal value λ^{STEP} satisfying an Euler-Lagrange equation. Relating to our work, as $t_f \rightarrow 0$, we have $\rho(x, t) \rightarrow \rho_i(x)$, and $\pi(x, t) \rightarrow 0$. The value of λ^{STEP} is what solves (20) with $\rho = \rho_i$ and $\pi = 0$.

Plugging $\rho = \rho_i \propto \exp(-(U_0 + \lambda_i U_1))$ and $\pi = 0$ into (20), we get

$$\lambda^{\text{STEP}} = \frac{\lambda_i + \lambda_f}{2}. \quad (47)$$

This is consistent with equations (S5) and (S7) of [10], but furthermore claims that for all potentials of the form (19), the optimal λ^{STEP} is the arithmetic mean of λ_i and λ_f .

For discretized space and time, we find λ^{STEP} that satisfies (11) for $\boldsymbol{\rho} = \boldsymbol{\rho}_i$ and $\boldsymbol{\pi} = \mathbf{0}$, and thus we obtain the fast protocol

$$\{\lambda_n^{\text{fast}} = \lambda^{\text{STEP}} \mid n = 1, \dots, N\}. \quad (48)$$

B.1.4 Slow protocol

In the slow, linear-response regime, as studied in [11], the amount of excess work for a differential amount of time Δt is given by

$$\Delta W_{\text{ex}} = \xi(\lambda) \dot{\lambda}^2 \Delta t \quad (49)$$

where $\xi(\lambda)$ is the friction tensor (a scalar for a one-dimensional parameter space) given by

$$\xi(\lambda) = \beta \int_0^\infty dt \langle \Delta U_1(0) \Delta U_1(t) \rangle_0. \quad (50)$$

Here, given our form of U_λ in (19), we have identified the conjugate force to λ as U_1 .

According to [12, 13], we can calculate the friction tensor using an eigendecomposition as

$$\xi(\lambda) = \beta \int dx \rho_\lambda(x) (U_1(x) - \langle U_1 \rangle_0) \sum_{k=1}^{\infty} u_k \frac{\phi_k(x)}{\epsilon_k} \quad (51)$$

where $\rho_\lambda(x) \propto \exp(-U_\lambda)$ is the equilibrium distribution of λ ; ϕ_k is the k th eigenvector of $\mathcal{L}_\lambda^\dagger$ with eigenvector $-\epsilon_k$, i.e. $\mathcal{L}_\lambda^\dagger \phi_k = -\epsilon_k \phi_k$, with ordering $\epsilon_0 = 0 < \epsilon_1 < \epsilon_2 < \dots$; and u_k is the coefficient of the decomposition $U_1(x) = \sum_{k=0} u_k \phi_k(x)$. For our simulations with spatial discretization, this integral over x becomes a discrete sum over the vector components of d states for each vector, with the eigendecomposition (ϕ_k, ϵ_k) calculated for matrix \mathcal{L}_λ^T from (2).

Given the form of (49), an optimal protocol in the linear response regime is given by a geodesic $\lambda^{\text{slow}}(t)$ where $\dot{\lambda}^{\text{slow}}(t) \propto \xi^{-1/2}(\lambda^{\text{slow}})$, with $\lambda^{\text{slow}}(0) = \lambda_i$ and $\lambda^{\text{slow}}(t_f) = \lambda_f$. To then numerically calculate the time-discretized slow protocol, we first define the protocol defined on time points $\{\lambda'_n \mid n = 0, 1, \dots, N; \lambda'_0 = \lambda_i, \lambda'_N = \lambda_f\}$ with λ'_n corresponding t_n , and we solve for the value of proportionality constant α so that

$$\lambda'_{n+1} - \lambda'_n = \alpha h_{n+1} \xi^{-1/2} \left(\frac{\lambda'_{n+1} + \lambda'_n}{2} \right). \quad (52)$$

Finally, we obtain slow protocol as the average between points

$$\left\{ \lambda_n^{\text{slow}} = \frac{\lambda'_{n+1} + \lambda'_n}{2} \mid n = 1, \dots, N \right\}. \quad (53)$$

B.2 W_{ex} calculation

The excess work $W_{\text{ex}}[\lambda(t)]$ of a protocol $\lambda(t)$ specifies how much more work is expended than the reversible work needed to do so adiabatically. It is non-negative by the second law of thermodynamics, and given by $W_{\text{ex}}[\lambda(t)] = W[\lambda(t)] - \Delta F$, where ΔF is the protocol-independent equilibrium free energy difference between the initial and final equilibrium states [14].

Numerically, given a specified protocol $\{\lambda_n\}$, to get the excess work $W_{\text{ex}}[\{\lambda_n\}]$, we first calculate the time evolution $\{\rho_n\}$ through

$$\begin{aligned} \rho_0 &= \rho_{\text{eq},i} \\ \rho_{n+1} &= e^{h_{n+1} \mathcal{L}_\lambda} \rho_n \Big|_{\lambda=\lambda_{n+1}}, \end{aligned}$$

and then the time-discretized version of (5):

$$W[\{\lambda_n\}] = (\mathbf{U}_f - \mathbf{U}_i)^T \rho_{\text{eq},i} + \sum_{n=0}^{N-1} \left[-(\mathbf{U}_\lambda - \mathbf{U}_f)^T (e^{h_{n+1} \mathcal{L}_\lambda} - \mathbb{1}) \rho_n \right]_{\lambda=\lambda_{n+1}}. \quad (54)$$

The protocol-independent discretized free energy is given by

$$\Delta F = -\log \left(\frac{\sum_k \exp(-[U_f]_k)}{\sum_k \exp(-[U_i]_k)} \right). \quad (55)$$

The excess work is then given by the difference between (54) and (55) as $W_{\text{ex}}[\{\lambda_n\}] = W[\{\lambda_n\}] - \Delta F$.

B.3 Discretization parameters and iterations-till-convergence

For the discretization of space of our numerical quartic examples, we use $\Delta x = 0.025$ with $x_b = 3$. For time discretization, we used $N = 1000$ time steps, considering both even timesteps $\{t_n = (n/(N+1))t_f \mid n = 0, 1, \dots, N\}$ and variable timesteps $\{t_n \mid n = 0, 1, \dots, N; \lambda^{\text{slow}}(t_n) = \lambda_i + (n/(N+1))(\lambda_f - \lambda_i)\}$. The variable time discretization was chosen because for the linearly biased double-well problem, both slow and optimal protocols have very steep slopes at the beginning and end of the protocols, for large t_f values; necessarily, for large t_f , a finer time discretization is needed for the beginning and end of the protocols for more accurate numerical convergence.

As a sanity check, we numerically calculated the optimal protocol for the variable stiffness harmonic oscillator problem, using spatial discretization $\Delta x = 0.025$, $x_b = 5$ and the abovementioned $N = 1000$ even and variable time discretizations. We considered $(\lambda_i = 1, \lambda_f = 2)$ and $(\lambda_i = 1, \lambda_f = 5)$, for a variety of t_f . Figure A.1 gives the corresponding numerical solutions for these cases. Comparing the numerically obtained protocol with the analytic solution (27), which is plotted in lighter-colored solid lines for each t_f , we see a very close match, with typical root-mean-squared error value 10^{-5} , never exceeding 1.8×10^{-3} (we get larger RMS error values for larger t_f , as the time step $\Delta t \approx t_f/N$ is generally larger). The closeness between the numerical and analytic solutions suggests a sufficiently fine discretization of space and time.

In calculating the optimal protocol, viewing a forward-backward sweep as a fixed point iteration, to accelerate the convergence of solution we used Anderson Acceleration [15, 16] with the additional parameters: restarts at $m = 30$, and relaxation $\beta = 0.5$ [17]. Convergence was determined when the root-mean-squared distance between two iterations of $\{\lambda_n\}$ was less than 10^{-8} . Interestingly, the number of fixed point iterations needed till convergence was roughly monotonic in t_f , as is displayed in Figure A.2. Despite the optimal protocol asymptoting to the slow protocol for large t_f (see Figures 1, 2, and A.1) and that the slow protocol used to initialize the forward-backward sweep algorithm, calculating the optimal protocol for larger t_f values required more iterations until convergence. This may not be too big of an issue, in that for the larger t_f regime ($t_f \gtrsim 20$) we can assume the slow protocol as being optimal (as is illustrated in Figures 1, 2, and A.1), eschewing the large number of forward-backward sweep iterations needed.

Our implementation was written in Python with the JIT compiler Numba [18], with each iteration taking around 2 minutes of real time to run on a single node of UC Berkeley’s Savio computational cluster. For coarser-grained time step, the number of iterations needed till convergence was independent of N on average, and gave a saving in runtime inversely proportional to N (e.g. around 15 seconds per iteration for $N = 100$, which in most cases was sufficient to demonstrate the above numerical results).

Appendix C Linear-in-time barrier crossing under full control

Here we show that for the optimal work-minimizing protocol under full control, the probability distribution is escorted so that the mean position changes at a constant rate

$$\frac{d\langle x \rangle}{dt} = \frac{d}{dt} \int \rho(x, t) x dx = \text{constant}. \quad (56)$$

We observed that the time-evolution of the probability density under the optimal protocol for the partial-control linearly biased double-well problem approximates this, and very closely for most E_0, t_f regimes, as depicted in Figures 3a and 3b. Our sketch derivation relies on results from optimal transport theory, and recent connections drawn for the entropy production-minimizing optimal protocols.

It may be shown [19, 20, 21, 22] that the excess dissipation $Q_{\text{ex}} = W_{\text{ex}} = W - \Delta F$ may be written as

$$Q_{\text{ex}} = \int dt \int dx \rho(x, t) v(x, t)^2 \quad (57)$$

where v is given by

$$v(x, t) = -\partial_x [\log(\rho(x, t)) + U(x, t)]. \quad (58)$$

as to reproduce Fokker-Planck dynamics

$$\partial_t \rho + \partial_x (\rho v) = 0. \quad (59)$$

For the full-control entropy-minimizing problem with $\rho(x, 0) = \rho_i(x)$ and $\rho(x, t_f) = \rho_f(x)$ specified (i.e. the first optimization problem described in the Introduction), finding the optimal protocol is akin to solving the optimal transport problem

$$Q_{\text{ex}}^* = \min_{v(x, t)} \int_0^{t_f} dt \int dx \rho(x, t) v(x, t)^2. \quad (60)$$

Through results from optimal transport theory [23], the optimal solution for (60) (i.e. the dynamical optimal coupling) gives the optimal value

$$Q_{\text{ex}}^* = \frac{\mathcal{W}(\rho_i, \rho_f)^2}{2t_f} \quad (61)$$

where $\mathcal{W}(\rho_i, \rho_f)^2$ is the L^2 -Wasserstein metric; that the instantaneous incurred excess heat is constant

$$\frac{dQ_{\text{ex}}^*}{dt} = \int dx \rho^*(x, t) v^*(x, t)^2 = \text{constant} \quad (62)$$

for all $t \in [0, t_f]$; and, crucially for our derivation, that

$$\frac{d\langle x \rangle}{dt} = \frac{d}{dt} \int dx \rho^*(x, t) x dx = \text{constant} \quad (63)$$

for all $t \in [0, t_f]$, as the underlying dynamical optimal coupling between $\rho_i(x)$ and $\rho_f(x)$ consists solely of constant-velocity curves in Euclidean space [23].

For the work-minimizing problem (i.e. the second optimization problem described in the Introduction, and what we consider in the paper for the partial-control case), we have $\rho(x, 0) = \rho_i(x)$, $U(x, 0) = U_i(x)$, and $U(x, t_f) = U_f(x)$ specified, with $\rho(x, t_f)$ unconstrained. The quantity W_{ex} to minimize can be written with an additional term

$$W_{\text{ex}}^* = \min_{\substack{v(x,t) \\ t \in [0, t_f]}} \left[\int_0^{t_f} dt \int dx \rho(x,t) v(x,t)^2 + \int_{t_f}^{\infty} dt \int dx \rho(x,t) v_f(x,t)^2 \right] \quad (64)$$

where

$$v_f(x,t) = -\partial_x [\log(\rho(x,t)) + U_f(x)], \quad (65)$$

fully specified by $U_f(x)$. The second term of (64), which corresponds to the dissipation as $\rho(x, t_f)$ relaxes to the equilibrium distribution of U_f post-protocol, is fully specified by $\rho(x, t_f)$ at time t_f , as v is set to v_f without variation for $t > t_f$.

In general, optimal solution $v^*(x, t)$ is different from the finite-time entropy minimization problem (60), by the virtue of the existence of the second term in (64). However, given the optimal solution $\{v^*(x, t), \rho^*(x, t)\}$ for (64), we have that $v^*(x, t)$ is identical to the solution of the entropy-minimization problem (60) with the same $\rho_i(x)$ initial condition and specified $\rho_f(x) = \rho^*(x, t_f)$ terminal condition; otherwise, there would be different $v^*(x, t)$ leading to the same $\rho^*(x, t_f)$, with a smaller value of the first term of (64).

Thus, one can conclude that for a work-minimizing optimal protocol with full control, the expected position is escorted with constant speed

$$\frac{d\langle x \rangle}{dt} = \frac{d}{dt} \int \rho^*(x, t) x dx = \text{constant} \quad (66)$$

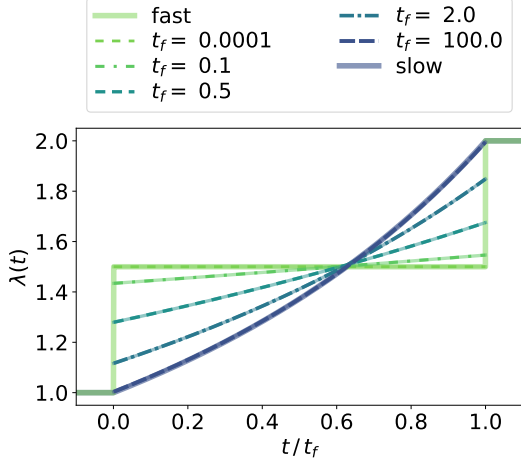
for all $t \in [0, t_f]$.

Insofar as a partial-control optimal protocol approximates the full-control optimal protocol, it should be the case that

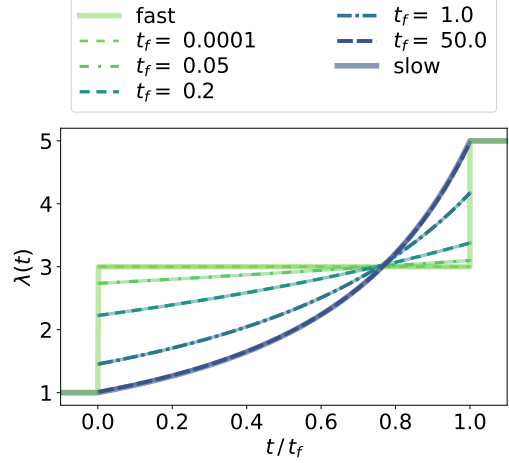
$$\frac{d\langle x \rangle}{dt} \approx \text{constant}, \quad (67)$$

even if requiring the optimal protocol to be non-monotonic, as in the case of $E_0 \sim 16, t_f \sim 0.2$ for the limited-control biased double-well problem.

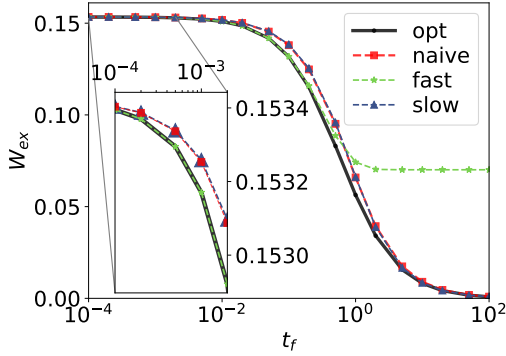
Eq. (67) is an exact equality for the analytic solution of a moving harmonic trap, as the average position evolves linearly in time (36) under the optimal protocol. We see in Figures 3a and 3b that for the linearly biased double-well problem, the mean $\langle x \rangle(t)$ of the probability distribution travels with near-constant velocity under the optimal protocol.



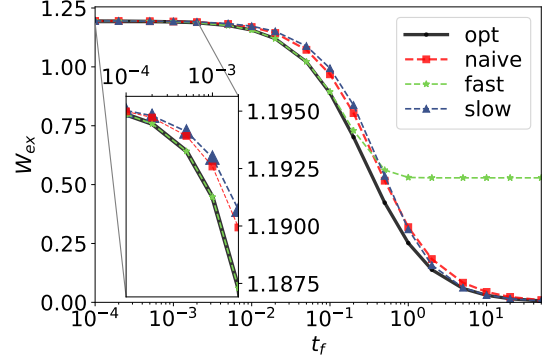
(a) Optimal protocol, $\lambda_i = 1, \lambda_f = 2$



(b) Optimal protocol, $\lambda_i = 1, \lambda_f = 5$



(c) Performance, $\lambda_i = 1, \lambda_f = 2$



(d) Performance, $\lambda_i = 1, \lambda_f = 5$

Figure A.1: Numerical results for the harmonic oscillator $U_\lambda(x) = \lambda x^2/2$, for $\lambda_i = 1, \lambda_f = 2$ (left column), and $\lambda_i = 1, \lambda_f = 5$ (right column). Unlike the quartic and double-well cases, we have the analytical solutions given by $\lambda(t) = (\lambda_i - \phi_i(1 + \phi_i t))/(1 + \phi_i t)^2$ with $\phi_i = (-(1 + \lambda_f t_f) + \sqrt{1 + 2\lambda_i t_f + \lambda_i \lambda_f t_f^2})/(2t_f + \lambda_f t_f^2)$, which are plotted in transparent bold for each t_f value. We see a very close fit between the numerically calculated optimal protocols and the analytical solutions in (a) and (b), with a typical root-mean-squared error value of 10^{-5} due to quantization noise. The performance of the optimal protocol exceeds that of the other protocols in (c) and (d). In many ways, the quartic case in Figure 1 is qualitatively similar to the harmonic case in both the form and performance of the optimal protocol.

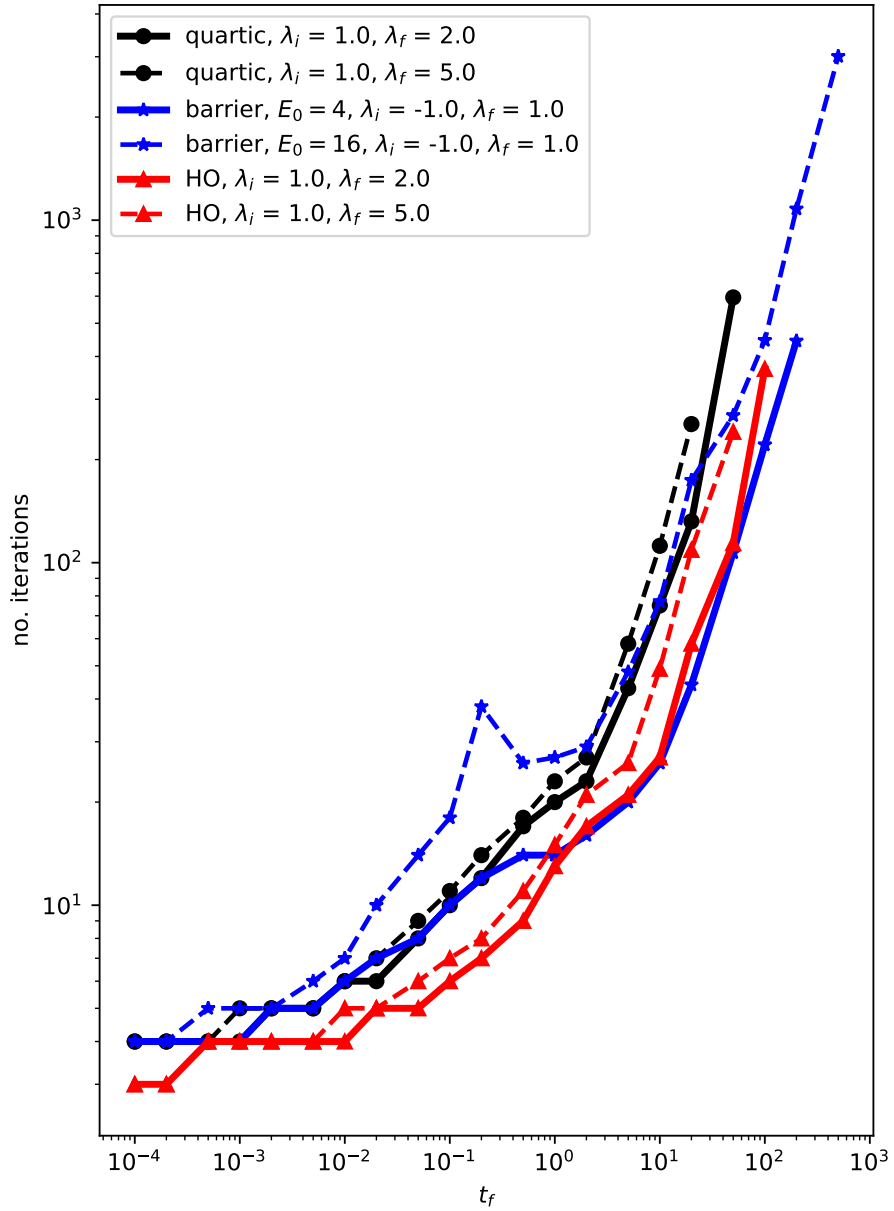


Figure A.2: Number of forward backwards sweep iterations under Anderson Acceleration needed for convergence for the optimal protocols displayed in Figures 1, 2, and A.1. We see that the number of iterations needed grows roughly monotonic with t_f , with the sole exception of the biased double-well problem at $t_f = 0.2$. Apparently, due to the non-monotonicity of the optimal protocol for $t_f = 0.2$ as displayed in Figure 2b, it takes more iterations for the candidate $\{\lambda^{(k)}\}$ to relax to the non-monotonic optimal protocol from its initialized value $\{\lambda^{(0)}\} = \{\lambda^{\text{slow}}\}$.

Appendix References

- [1] Tim Schmiedl and Udo Seifert. “Optimal finite-time processes in stochastic thermodynamics”. In: *Physical review letters* 98.10 (2007), p. 108301.
- [2] Viktor Holubec, Klaus Kroy, and Stefano Steffenoni. “Physically consistent numerical solver for time-dependent Fokker-Planck equations”. In: *Physical Review E* 99.3 (2019), p. 032117.
- [3] Hannes Risken. “Fokker-planck equation”. In: *The Fokker-Planck Equation*. Springer, 1996, pp. 63–95.
- [4] Robert Zwanzig. *Nonequilibrium statistical mechanics*. Oxford university press, 2001.
- [5] Michael McAsey, Libin Mou, and Weimin Han. “Convergence of the forward-backward sweep method in optimal control”. In: *Computational Optimization and Applications* 53.1 (2012), pp. 207–226.
- [6] Suzanne Lenhart and John T Workman. *Optimal control applied to biological models*. Chapman and Hall/CRC, 2007.
- [7] Marlis Hochbruck and Christian Lubich. “Exponential integrators for quantum-classical molecular dynamics”. In: *BIT Numerical Mathematics* 39.4 (1999), pp. 620–645.
- [8] Dominik L Michels and Mathieu Desbrun. “A semi-analytical approach to molecular dynamics”. In: *Journal of Computational Physics* 303 (2015), pp. 336–354.
- [9] Henghsiu Tsai and KS Chan. “A note on parameter differentiation of matrix exponentials, with applications to continuous-time modelling”. In: *Bernoulli* 9.5 (2003), pp. 895–919.
- [10] Steven Blaber, Miranda D Louwerse, and David A Sivak. “Steps Minimize Dissipation in Rapidly Driven Stochastic Systems”. In: *arXiv preprint arXiv:2105.04691* (2021).
- [11] David A Sivak and Gavin E Crooks. “Thermodynamic metrics and optimal paths”. In: *Physical review letters* 108.19 (2012), p. 190602.
- [12] Neha S Wadia, Ryan V Zarcone, and Michael R DeWeese. “Solution to the Fokker-Planck equation for slowly driven Brownian motion: Emergent geometry and a formula for the corresponding thermodynamic metric”. In: *Physical Review E* 105.3 (2022), p. 034130.
- [13] Adrienne Zhong and Michael R. DeWeese. “Eigendecomposition calculation of friction tensor”. In: (Forthcoming).
- [14] Christopher Jarzynski. “Nonequilibrium equality for free energy differences”. In: *Physical Review Letters* 78.14 (1997), p. 2690.
- [15] Jesse A Sharp, Kevin Burrage, and Matthew J Simpson. “Implementation and acceleration of optimal control for systems biology”. In: *Journal of the Royal Society Interface* 18.181 (2021), p. 20210241.
- [16] Yue Peng et al. “Anderson acceleration for geometry optimization and physics simulation”. In: *ACM Transactions on Graphics (TOG)* 37.4 (2018), pp. 1–14.
- [17] Nicholas C Henderson and Ravi Varadhan. “Damped Anderson acceleration with restarts and monotonicity control for accelerating EM and EM-like algorithms”. In: *Journal of Computational and Graphical Statistics* 28.4 (2019), pp. 834–846.
- [18] Siu Kwan Lam, Antoine Pitrou, and Stanley Seibert. “Numba: A llvm-based python jit compiler”. In: *Proceedings of the Second Workshop on the LLVM Compiler Infrastructure in HPC*. 2015, pp. 1–6.
- [19] Andreas Dechant and Yohei Sakurai. “Thermodynamic interpretation of Wasserstein distance”. In: *arXiv preprint arXiv:1912.08405* (2019).

- [20] Muka Nakazato and Sosuke Ito. “Geometrical aspects of entropy production in stochastic thermodynamics based on Wasserstein distance”. In: *arXiv preprint arXiv:2103.00503* (2021).
- [21] Yongxin Chen, Tryphon T Georgiou, and Allen Tannenbaum. “Stochastic control and nonequilibrium thermodynamics: Fundamental limits”. In: *IEEE transactions on automatic control* 65.7 (2019), pp. 2979–2991.
- [22] Shriram Chennakesavalu and Grant M. Rotskoff. *Unifying thermodynamic geometries*. 2022. arXiv: 2205.01205 [cond-mat.stat-mech].
- [23] Cédric Villani. *Optimal transport: old and new*. Vol. 338. Springer, 2009.